Coherent backscattering of polarized light for tissue diagnostics: an Electric field Monte Carlo study

Min Xu

Department of Physics, Fairfield University, 1073 North Benson Road, Fairfield, CT 06824
Email: mxu@mail.fairfield.edu

ABSTRACT

We report on a novel Electric field Monte Carlo (EMC) approach for directly simulating coherent backscattering (CBS) of coherent or partially coherent polarized light. The strong dependence of CBS on the polarization state of light is first demonstrated. The penetration depth of low coherence backscattering light is then investigated using the EMC approach. EMC simulations of linearly polarized light backscattering from a human epithelial tissue model show that the penetration depth of low coherence backscattering light is reduced to the level of one scattering length under illumination by a source of an extreme low spatial coherence. The penetration depth less than one scattering length has not been obtained even when the spatial coherence length is shortened to be one percent of the scattering mean free path. It is found that the penetration depth of low coherence backscattering light may remain orders of magnitude larger than the spatial coherence length of the partially coherent source when the coherence length is shortened in an attempt to shrink the probing depth of light. This calls for a careful interpretation of the penetration depth for low coherence backscattering techniques applied to tissue diagnostics.

Keywords: Electric field Monte Carlo, coherent backscattering, penetration depth, tissue diagnostics, turbid medium, low coherence backscattering

1. INTRODUCTION

Coherent backscattering (CBS) of light is one intriguing phenomenon which manifests itself as a sharp peak of intensity centered at exactly the backscattering direction for an incident coherent beam owing to the constructive interference between coherent waves traveling in a pair of time-reversed trajectories.[1–3] The enhancement may reach a factor of two close to the exact backscattering direction compared to backscattering of incoherent light. The enhancement profile can be used to probe the optical properties of the subsurface of highly scattering media. This technique is, in particular, effective in probing the superficial layer of tissues and has been shown to be sensitive to cancerous changes in epithelial cells. It is, however, a challenge to model CBS as (1) non-diffusive photons contribute appreciably to CBS, and (2) the enhancement profile depends strongly on both the polarization and coherent state of light. Most current investigations on CBS have relied on an indirect approach (CBS is approximated by a Fourier transform of the spatial distribution of backscattered incoherent light) based on Monte Carlo simulations and are limited to scalar light.[4]

In this paper, we first report on a novel Electric field Monte Carlo (EMC) approach for directly simulating coherent backscattering of coherent or partially coherent polarized light. In EMC, electric field, in contrast to a Stokes vector, is traced in simulation. The electric fields of backscattered coherent waves traveling in a pair of time-reversed trajectories are added coherently to produce their interference effect. This presents a clean, intuitive and efficient approach to model CBS. We first demonstrate the strong dependence of CBS on the polarization state of light. The penetration depth of low coherence backscattering light applied to probe biological samples is then studied by EMC simulations. The simulation results on linearly polarized partially coherent light backscattering from a human epithelial tissue model show the penetration depth of low coherence backscattering light reduces with the decrease of the spatial coherence length. Yet the penetration depth is still larger than one scattering mean free path l_s even when the spatial coherence length is shortened to $0.01 l_s$.

Optical Interactions with Tissue and Cells XIX, edited by Steven L. Jacques, William P. Roach, Robert J. Thomas,
Proc. of SPIE Vol. 6854, 68541A, (2008) · 1605-7422/08/$18 · doi: 10.1117/12.762399

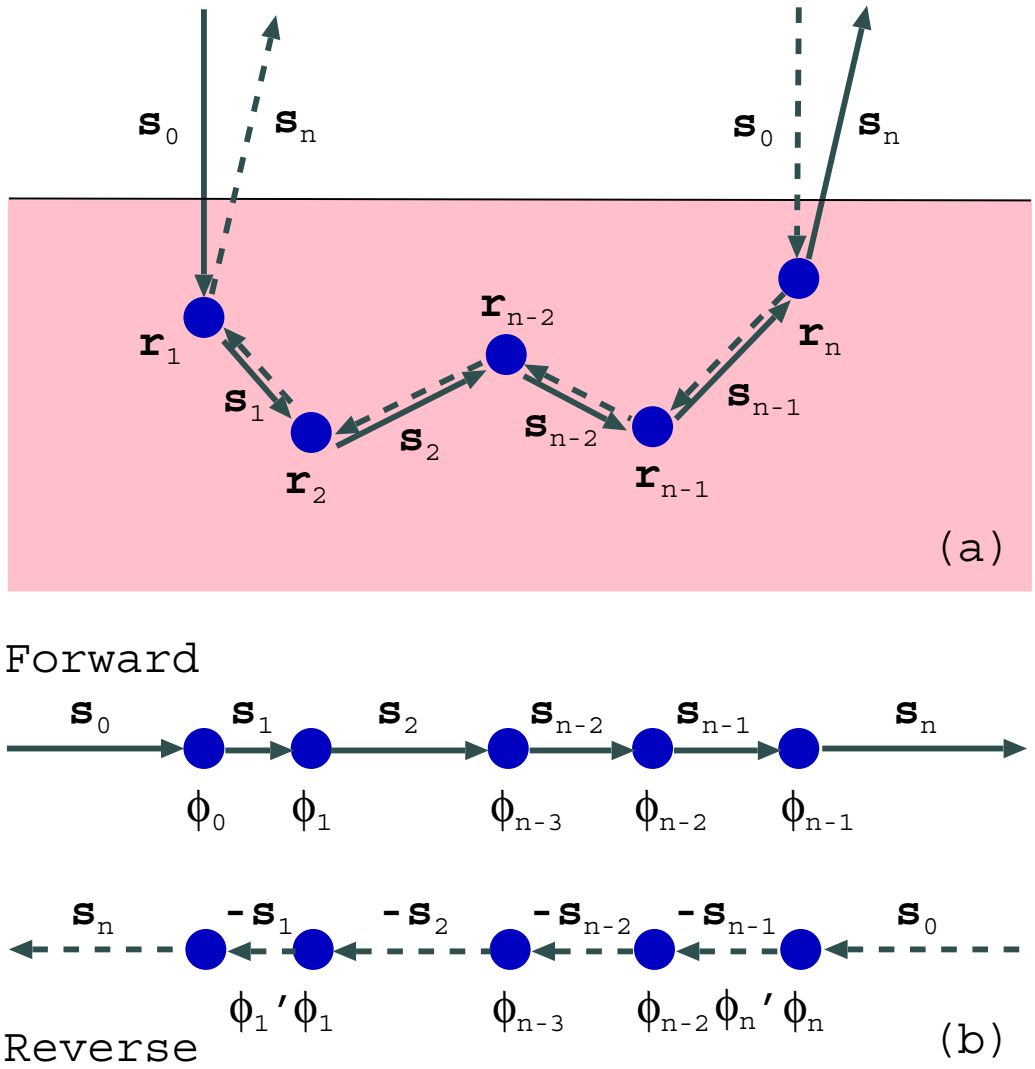

Figure 1. (a) Propagation of a pair of partial waves along the forward and reverse paths. (b) The azimuthal rotations of the local coordinate system along the forward and reverse paths.

2. ELECTRIC FIELD MONTE CARLO METHOD FOR SIMULATING COHERENT BACKSCATTERING OF POLARIZED LIGHT

We have extended Electric field Monte Carlo (EMC) method[5,6] for simulating coherent backscattering of polarized light from a turbid medium. Electric fields of partial waves traveling in a pair of time-reversed paths are added coherently to simulate their interference, taking into full account their amplitude and phase difference from multiple scattering when traveling in the pair of paths in opposite orders. Such an extra phase difference than that from their optical path difference is a pure result of the vector nature of light. EMC simulation results manifest the importance of this vector phase difference and point out serious errors may result in interpreting CB based on models neglecting this effect.

The propagation of light in a turbid medium is formulated as a series of update of the parallel and perpendicular polarized electric components E_j $(j = 1, 2)$ with respect to the present scattering plane and a rotation of the local coordinate system spanned by $(\mathbf{m}, \mathbf{n}, \mathbf{s})^T$ where $\mathbf{m}$, $\mathbf{n}$, and $\mathbf{s}$ represent the unit vectors in the directions of parallel polarization, perpendicular polarization, and propagation, respectively.[5,7] The electric field of light is given by the superposition of its two components $\mathcal{E} = E_1\mathbf{m} + E_2\mathbf{n}$.

Consider now a beam of light $\mathcal{E}_0$ incident along $\mathbf{s}_0$ enters a semi-infinite turbid medium and encounters a series of scattering at sites $\mathbf{r}_i$ ($i = 1, 2, \ldots, n$) before escaping the medium in the direction $\mathbf{s}_n$ (see Fig. 1). Denote the initial reference frame of the incident beam as $(\mathbf{m}_0, \mathbf{n}_0, \mathbf{s}_0)^T$, the local coordinate system as $(\mathbf{m}_i, \mathbf{n}_i, \mathbf{s}_i)^T$ and the amplitude scattering matrix as $S^{(i)}(\mathbf{s}_i, \mathbf{s}_{i-1})$, respectively, at the ith scattering at $\mathbf{r}_i$, ϕ_{i-1} as the azimuthal angle to rotate $\mathbf{n}_{i-1}$ to $\mathbf{n}_i$ about the axis $\mathbf{s}_{i-1}$, and θ_{i-1} as the scattering angle for light being scattered from $\mathbf{s}_{i-1}$ to $\mathbf{s}_i$. The unit vector $\mathbf{n}_i = \mathbf{s}_{i-1} \times \mathbf{s}_i / |\mathbf{s}_{i-1} \times \mathbf{s}_i|$ is the normal of the scattering plane spanned by $\mathbf{s}_{i-1}$ and $\mathbf{s}_i$ at the ith scattering event. The outgoing electric field in the forward path can be written as

$$\mathbf{E}_{\rm out} = S^{(n)}(\mathbf{s}_n, \mathbf{s}_{n-1}) R(\phi_{n-1}) T S^{(1)}(\mathbf{s}_1, \mathbf{s}_0) R(\phi_0) \mathbf{E}_0, \tag{1}$$

where $T = \prod_{i=2}^{n-1} S^{(i)}(\mathbf{s}_i, \mathbf{s}_{i-1}) R(\phi_{i-1})$ is an ordered product where terms of a larger index i is placed to the left of terms of a smaller index. The rotation matrix R is given by

$$R(\phi) = \begin{pmatrix} \cos\phi & \sin\phi \\ -\sin\phi & \cos\phi \end{pmatrix}. \tag{2}$$

The wave traveling in the reverse path is scattered at sites $\mathbf{r}_n$, $\mathbf{r}_{n-1}$, ..., and $\mathbf{r}_1$, sequentially in the opposite order than that in the forward path, with its propagation direction rotating from $\mathbf{s}_0$ to $-\mathbf{s}_{n-1}$, ..., to$-\mathbf{s}_1$, and finally escaping in $\mathbf{s}_n$ direction. The electric field in the backward path can be written as

$$\mathbf{E}^{\rm rev}_{\rm out} = S^{(1)}(\mathbf{s}_n, -\mathbf{s}_1) R(\phi_1') T^{\rm rev} R(\phi_n') S^{(n)}(-\mathbf{s}_{n-1}, \mathbf{s}_0) R(\phi_n) \mathbf{E}_0. \tag{3}$$

Here $R(\phi_n)$ is the rotation matrix which aligns $\mathbf{n}_0$ to the normal $\mathbf{n}' = \mathbf{s}_0 \times (-\mathbf{s}_{n-1}) / |\mathbf{s}_0 \times (-\mathbf{s}_{n-1})|$ of the scattering plane at the first scattering site, $\mathbf{r}_n$, in the reverse path; $R(\phi_n')$ aligns $\mathbf{n}'$ to, $-\mathbf{n}_{n-1}$, the normal of the scattering plane at the second scattering site, $\mathbf{r}_{n-1}$, in the reverse path; $T^{\rm rev} = \prod_{i=2}^{n-1} R(\phi_{i-1}) S^{(i)}(-\mathbf{s}_{i-1}, -\mathbf{s}_i)$ is an ordered product where terms of a larger index i is placed to the right of terms of a smaller index, which represents light being scattered by sites $\mathbf{r}_{n-1}$, $\mathbf{r}_{n-2}$,. . .,$\mathbf{r}_2$ sequentially and the local coordinate system for light being rotated from $(\mathbf{m}_{n-1}, -\mathbf{n}_{n-1}, -\mathbf{s}_{n-1})^T$ to $(\mathbf{m}_1, -\mathbf{n}_1, -\mathbf{s}_1)^T$ after $(n-2)$ scattering events; and $R(\phi_1')$ is the rotation matrix which aligns $-\mathbf{n}_1$ to the normal $\mathbf{n}'' = -\mathbf{s}_1 \times \mathbf{s}_{\rm out} / |-\mathbf{s}_1 \times \mathbf{s}_{\rm out}|$ of the scattering plane at the last scattering site, $\mathbf{r}_1$, in the reverse path. The other quantities involved in the reverse path are the same as those in the forward path. The operator $T^{\rm rev}$ relates to T as $T^{\rm rev} = QT^TQ$ where $Q = {\rm diag}(1, -1)$ owing to the time-reversal symmetry of electromagnetic waves. [8]

In the special case when light is backscattered in the exact backscattering direction ($\mathbf{q}_b = k(\mathbf{s}_0 + \mathbf{s}_n) = 0$), $\mathbf{E}^{\rm rev}_{\rm out}$ can be simplified as $R(\phi_1') = 1$ and $R(\phi_n') = R(\phi_{n-1})$. If one further rotates the local coordinate systems for $\mathbf{E}_{\rm out}$ and $\mathbf{E}^{\rm rev}_{\rm out}$ to $(\mathbf{m}_0, -\mathbf{n}_0, -\mathbf{s}_0)^T$, the electric field in the forward and the reversed paths can be written as $\mathbf{E}_{\rm out} = \mathcal{T}\mathbf{E}_0$ and $\mathbf{E}^{\rm rev}_{\rm out} = \mathcal{T}^{\rm rev}\mathbf{E}_0$ where $\mathcal{T} = R(\phi_n) S^{(n)}(\mathbf{s}_n, \mathbf{s}_{n-1}) R(\phi_{n-1}) T S^{(1)}(\mathbf{s}_1, \mathbf{s}_0) R(\phi_0)$ and $\mathcal{T}^{\rm rev} = Q\mathcal{T}^TQ$. Inside the polarization preserved channels, the phase difference between the two partial waves $\mathbf{E}_{\rm out}$ and $\mathbf{E}^{\rm rev}_{\rm out}$ can be found to be zero. It is, however, not true for polarization unpreserved channels even when $\mathbf{q}_b = 0$. For example, $\mathbf{E}_{\rm out} = \mathcal{T}_{11} E_0 \hat{x} + \mathcal{T}_{21} E_0 \hat{y}$ and $\mathbf{E}^{\rm rev}_{\rm out} = \mathcal{T}_{11} E_0 \hat{x} - \mathcal{T}_{12} E_0 \hat{y}$ for an incident x polarized beam $\mathbf{E}_0 = E_0 \hat{x}$ where $\mathcal{T}_{ij}$ is the (i, j)-th element of the 2×2 matrix $\mathcal{T}$. The outgoing electric fields are guaranteed to have the common phase in the polarization preserved (x polarization) channel and are not so in the polarization unpreserved (y polarization) channel. The phases (and magnitudes) of $\mathbf{E}_{\rm out}$ and $\mathbf{E}^{\rm rev}_{\rm out}$ are, in general, inherently different due to the vector nature of light. This is the reason why CBS obtained by a Fourier transform of the spatial distribution of backscattered incoherent light is limited to the case of scalar light and can produce uncontrollable errors in the case of polarized light because the additional phase difference owing to light depolarization is not taken into account there. This issue will be examined further elsewhere.

The EMC method for simulating CB uses Eqs. (1) and (3) to compute the electric field traveling along a pair of time-reversed paths. The intensity of the coherent backscattered light is obtained from $|\mathbf{E}_{\rm out} + \mathbf{E}^{\rm rev}_{\rm out} \exp(i\delta)|^2$ where $\delta \equiv \mathbf{q}_b \cdot (\mathbf{r}_n - \mathbf{r}_1)$ is the phase delay introduced by the optical path difference. The backscattered light encountering only one scattering is computed separately. A partial photon technique [4] is used to improve the efficiency of the EMC simulation. When the incident light is partially coherent, the following quantity is computed

$$|\mathbf{E}_{\rm out}|^2 + |\mathbf{E}^{\rm rev}_{\rm out}|^2 + 2\Re\left[J \mathbf{E}^*_{\rm out} \mathbf{E}^{\rm rev}_{\rm out} \exp(i\delta)\right] \tag{4}$$

for the intensity of the coherent backscattered light where $\Re$ denotes the real part and the extra factor,

$$J = \left[2 \frac{J_1(\rho/L_c)}{\rho/L_c}\right]^2, \tag{5}$$

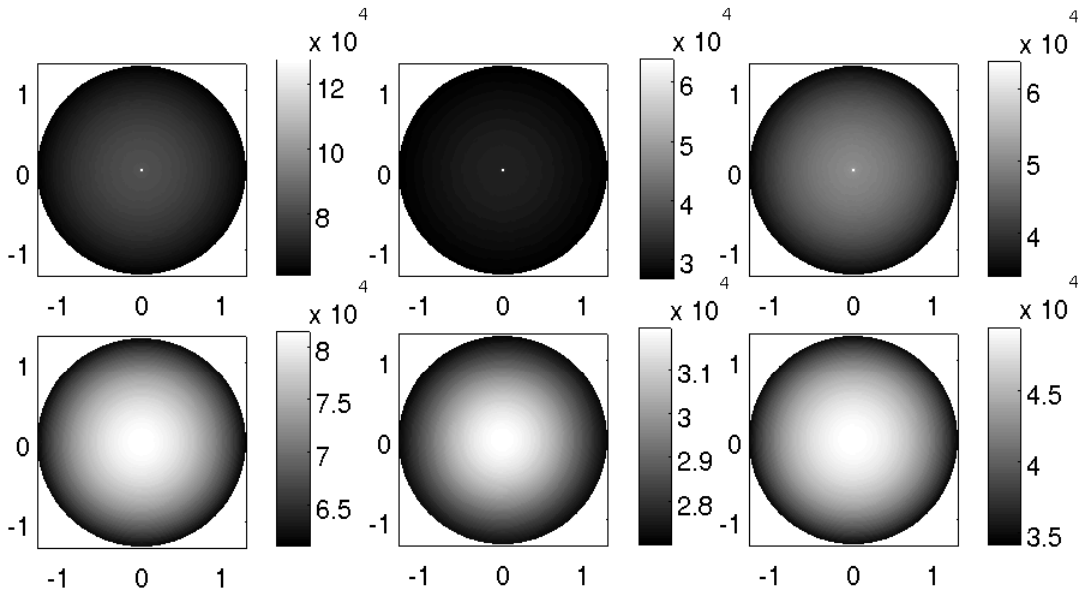

Figure 2. Backscattering of normally incident circularly polarized light. The first row displays $I_+ + I_-$, I_+, and I_- from left to right for incident coherent light; the bottom row displays the corresponding intensities for incident incoherent light. Each circle depicts the view around the exact backscattering direction where the zenith angle (in radian) is the circle's radius and the azimuthal angle is the polar angle.

comes from (1) the complex degree of coherence of a partially spatial coherent light of a circular shape with a radius $a \gg L_c$ (L_c is the coherence length) at the illumination points separated by a transversal distance of ρ,[9] and (2) the averaging of light over the illuminated area assuming the size of the illuminated area is much larger than L_c. The latter was ignored in some recent work,[10] resulting in an incorrect factor without the power 2.

3. RESULT

3.1. Dependence of coherent backscattering on polarization

We performed EMC simulations of coherent backscattering of normally incident circularly polarized light and linearly polarized light from a turbid medium. Each simulation used 125,000 photon packets using the partial photon technique and took less than twenty-four hours on a single 2.33 GHz Intel Xeon core to simulate the electric field in both the forward and reverse paths covering the backscattering directions at 73 azimuthal detection angles and 76 zenith detection angles. The turbid medium is composed of a water suspension of Mie scatterers whose diameter is 0.1 micrometers and refractive index is 1.58984. The wavelength of the incident light is 0.5145 micrometers. The thickness of the turbid medium is 20 scattering mean free paths.

Figure 2 illustrates coherent backscattering of normally incident circularly polarized light. The top row displays the backscattering intensities of incident coherent light of circular polarization (left: $I_+ + I_-$, middle: I_+, right: I_-). $I_\pm$ is the intensity of the backscattered light of the same (or opposite) helicity as that of the incident beam. The second row displays the corresponding intensities for incident incoherent light of circular polarization. As one can see from the figure, the intensity of backscattered light does not depend on the azimuthal angle as circularly polarized light has by definition centric symmetry.

Figure 3 illustrates the intensity of backscattered light for normally incident linearly polarized light around the exact backscattered direction. The first row in Figure 3 is, from left to right, backscattered $I_x + I_y$, I_x, and I_y for incident coherent light. The second row is the same except the incident light is incoherent. The third row is the same as the first row but the zenith detection angle goes from 0 degrees to 2.25 degrees instead of 75 degrees.

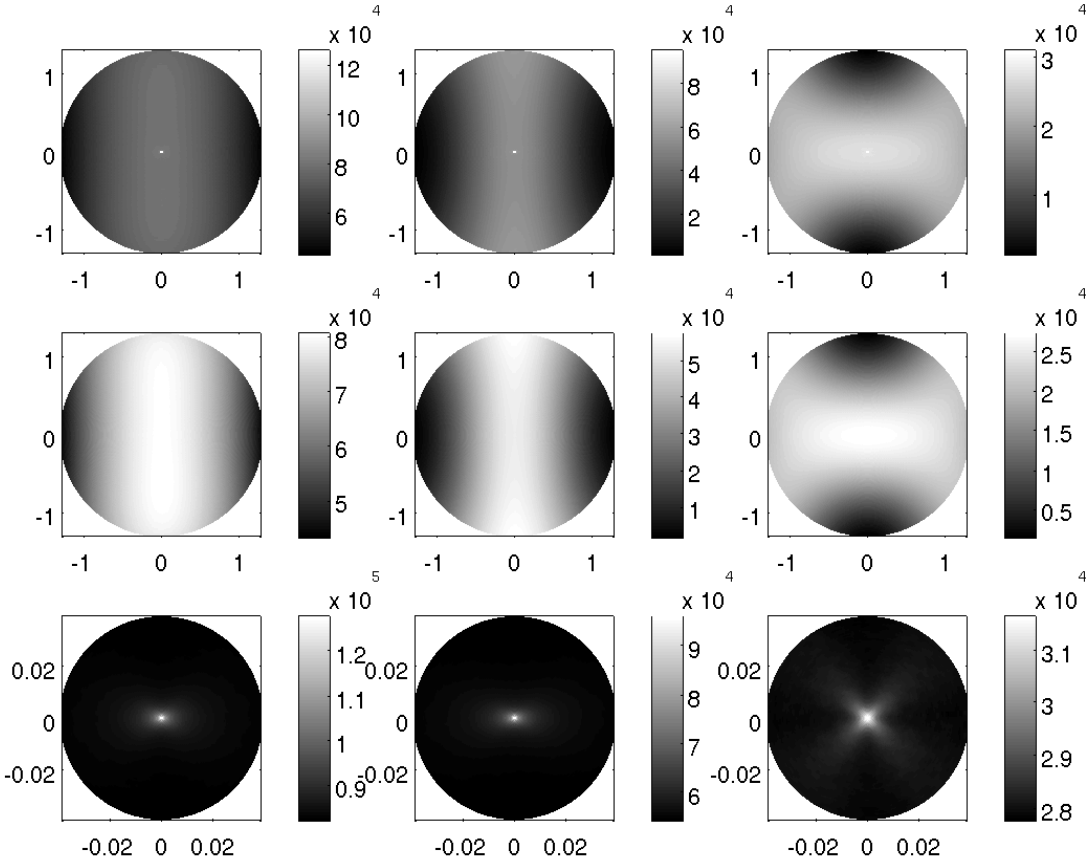

Figure 3. Backscattering of normally incident linearly polarized light. The incident beam is polarized linearly in the x-direction. Each circle depicts the view around the exact backscattering direction where the zenith angle (in radian) is the circle's radius and the azimuthal angle is the polar angle. The first row is, from left to right, backscattered $I_x + I_y$, I_x, and I_y for incident coherent light. The second row is the same except the incident light is incoherent. The third row is the same as the first row but the zenith detection angle goes from 0 degrees to 2.25 degrees instead of 75 degrees.

Unlike the case involving circularly polarized light, the intensity of backscattered light for an incident linearly polarized light is no longer circular symmetric. As to understand why the patterns for I_x are elongated along the y-axis and the patterns for I_y are elongated along the x-axis, we point out that light tends to be scattered preferably into directions out of the plane of its polarization when scattered by a Mie scatterer. Thus the x-component is elongated along the y-axis and squeezed in along the x-axis and the y-component is elongated along the x-axis and squeezed in along the y-axis. Closer to the exact backscattering direction (bottom row of Figure 3), backscattering of coherent linearly polarized light appears to display different symmetries. I_x appears to now be elongated along the x-axis and squeezed slightly at the y-axis owing to the much stronger enhancement factor for backscattered light remitting from along the x-axis. I_y also displays interesting 4-fold "X" symmetry closer to the exact escape direction, which is characteristic of light being multiply scattered by Rayleigh-like particles. Further details were presented elsewhere.[11]

3.2. Coherent backscattering from tissue: penetration depth vs spatial coherence length of incident beam

We applied EMC to investigate coherent backscattering of coherent or partially coherent light from tissue. Earlier studies suggest unified Mie and fractal model describes well light scattering by biological cells and tissues covering the whole visible spectra and from forward to backward scattering angles.[12–14] Based on that finding, we modeled tissue as a medium composed of large spherical scatterers and a background with random fluctuation in the refractive index. The size and the refractive index of the large scatterers were assumed to be $10\ \mu m$ and 1.400, respectively, to model enlarged nuclei due to carcinogenesis; the fractal dimension and the cutoff correlation length of the background refractive index fluctuation were $D_f = 4.68$ and $l_{\max} = 0.337\ \mu m$, respectively; and the background refractive index of the medium was assumed 1.360. The strength of the background refractive index fluctuation and the number density of the large spherical scatterers were adjusted to produce the ratio of Mie and fractal scattering, $\mu_{s,\mathrm{Mie}} : \mu_{s,\mathrm{bg}} = 15 : 1$, and the scattering mean free path $230\ \mu m$ at wavelength 630 nm.[15] The resulting anisotropy factor, $g = 0.975$, at wavelength 630 nm, is consistent with the measured value for epithelia.[16] In the simulation, the thickness of the medium is set to be $10 l_t = 10 l_s/(1-g)$ where l_t and l_s are the transport and scattering mean free paths, respectively. The wavelength of the incident linearly polarized light (polarization along the x direction) is 400 nm. The anisotropy factor is $g = 0.964$ at this wavelength. The transport and scattering mean free paths are $l_t = 4611\ \mu m$ and $l_s = 168\ \mu m$, respectively.

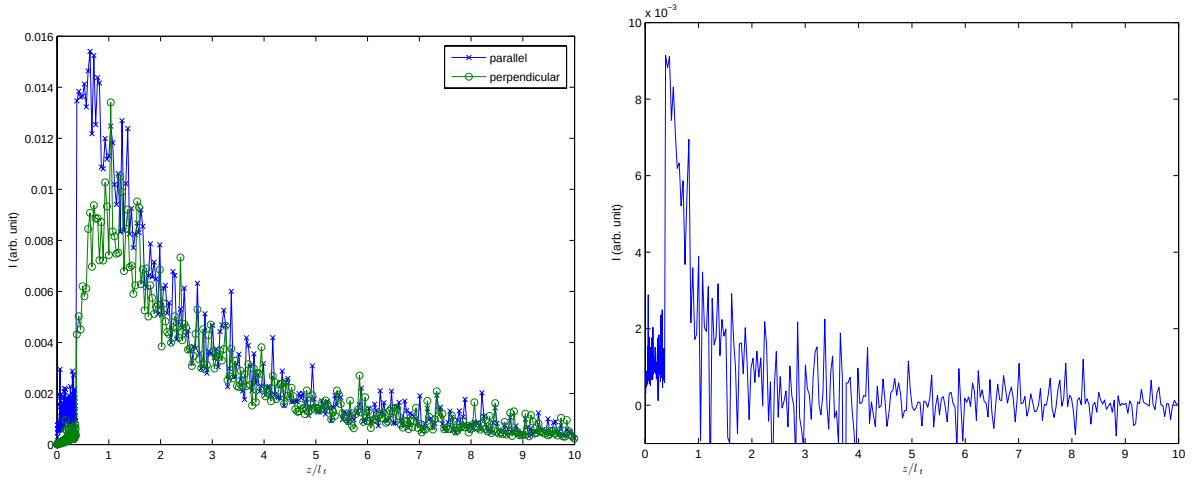

(a) (b)

Figure 4. (a) The distribution of photons of penetration depth $z_{\max}$ for backscattered incoherent light of parallel or perpendicular polarization in the exact backscattering direction. (b) The direction of photons of penetration depth $z_{\max}$ for their difference $(I_x - i_y)$ in the exact backscattering direction. Linearly polarized light polarized along x direction is normally incident on the medium.

Figure 4 shows the distribution of photons of penetration depth $z_{\max}$ for (a) backscattered incoherent light in the exact backscattering direction of parallel or perpendicular polarization and (b) their difference $(I_x - I_y)$ in the exact backscattering direction. The penetration depth and its variance for backscattered incoherent light are summarized in Table 1. The difference between parallel and perpendicular polarized backscattered light, $I_x - I_y$, has a reduced penetration depth at the level of one l_t.

Table 1. The penetration depth and its variance for backscattered incoherent light.

	I_x	I_y	$I_x - I_y$
$\langle z_{\max} \rangle$	$2.34 l_t$	$2.83 l_t$	$0.91 l_t$
$\sqrt{\langle \Delta z_{\max}^2 \rangle}$	$2.24 l_t$	$3.64 l_t$	$1.67 l_t$

Low coherence light can be used to reduce the penetration depth of light further. Figure 5 and Table 2 show the much reduced penetration depth for the backscattering of low coherence light. This low coherence light is the difference between the coherent backscattered light of parallel polarization and the incoherent background. The distributions of photons versus the maximum penetration depth for a few cases of varying spatial coherence length are displayed in Fig. 6. One surprising finding is that although the mean penetration depth tends to decrease with the shrinkage of the spatial coherence length, the penetration length stays above one l_s even for the case that the spatial coherence length is as low as $L_c = 0.01 l_s$. That is, even when $L_c = 1.7\ \mu m$, the penetration depth is still above $175\ \mu m$. This suggests that the penetration depth of low coherence light may be orders of magnitude larger than the spatial coherence length when L_c is shortened in an attempt to shrink the probing depth of light.

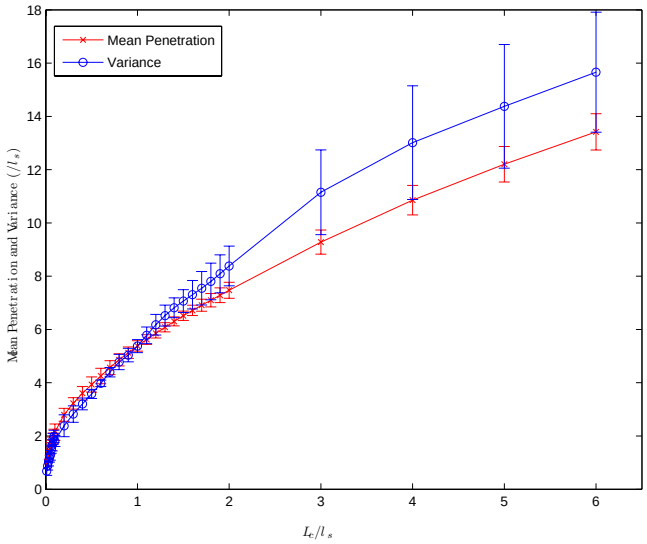

Figure 5. The penetration depth and its variance for backscattered low coherence light. Note the x axis plots $z_{\max}/l_s$ and $l_s = 0.0364 l_t$. The errorbars were computed from 6 independent EMC simulations.

Table 2. The penetration depth and its variance for low coherence backscattered light of parallel polarization.

L_c/l_s	0.01	0.02	0.05	0.1	0.5	1	2
$\langle z_{\max} \rangle / l_s$	1.04 ± 0.17	1.19 ± 0.17	1.54 ± 0.21	2.15 ± 0.31	3.93 ± 0.29	5.38 ± 0.20	7.47 ± 0.30
$\sqrt{\langle \Delta z_{\max}^2 \rangle}/l_s$	0.68 ± 0.15	0.87 ± 0.16	1.28 ± 0.18	1.81 ± 0.21	3.58 ± 0.17	5.38 ± 0.25	8.38 ± 0.74

The importance of double scattering versus multiple scattering (at least three scattering events) for the low coherence backscattering light is plotted in Fig. 7. Double scattering light is about 50% of the backscattered low coherence light when $L_c = 0.01 l_s$. The importance of the double scattering light goes down rapidly with the increase of L_c. Double scattering light is about $1/4$ and $1/8$ of the total backscattered low coherence light for $L_c = 0.1 l_s$and $L_c = 0.5 l_s$, respectively.

Finally, to corroborate with our earlier analysis, the distribution of photons reaching maximum penetration $z_{\max}$ for double scattered light is plotted in Fig. 8. The maximum penetration depth for double scattered light is $\langle z_{\max} \rangle = (0.84 \pm 0.02) l_s$, $\sqrt{\langle \Delta z_{\max}^2 \rangle} = (0.62 \pm 0.02) l_s$, $\langle z_{\max} \rangle = (0.95 \pm 0.02) l_s$, and $\sqrt{\langle \Delta z_{\max}^2 \rangle} = (0.68 \pm 0.01) l_s$ for the case of spatial coherence length of the source, $L_c = 0.01 l_s$ and $L_c = 0.1 l_s$, respectively.

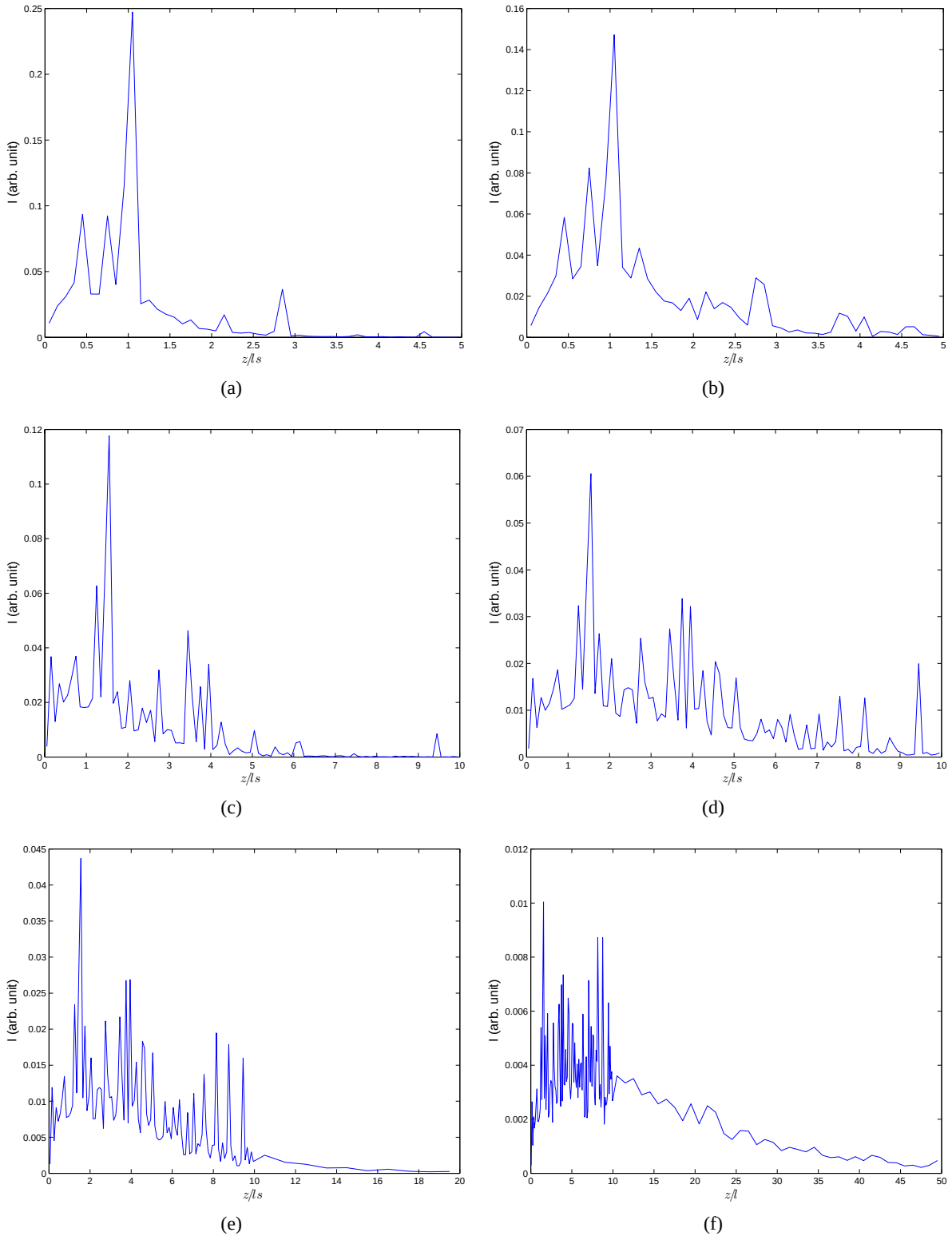

Figure 6. The distribution of photons of penetration depth $z_{\max}$ for backscattered low coherence light of parallel polarization in the exact backscattering direction. (a) $L_c = 0.01l_s$, (b) $L_c = 0.05l_s$, (c) $L_c = 0.1l_s$, (d) $L_c = 0.5l_s$, (e) $L_c = l_s$, and (f) $L_c = 0.5l_t = 13.7l_s$.

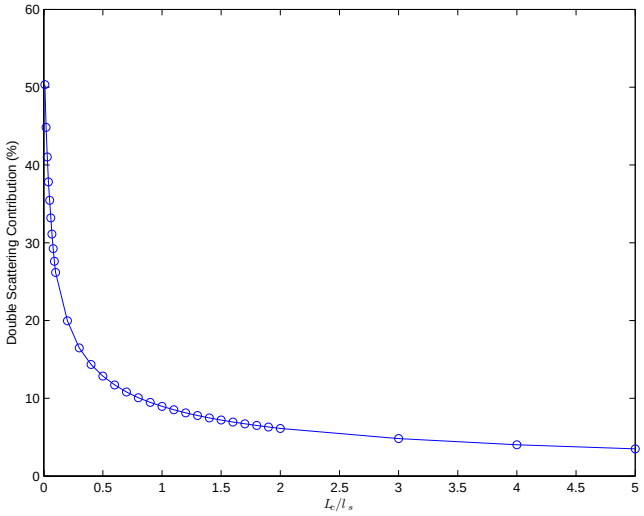

Figure 7. The importance of double scattering for the low coherence backscattered light.

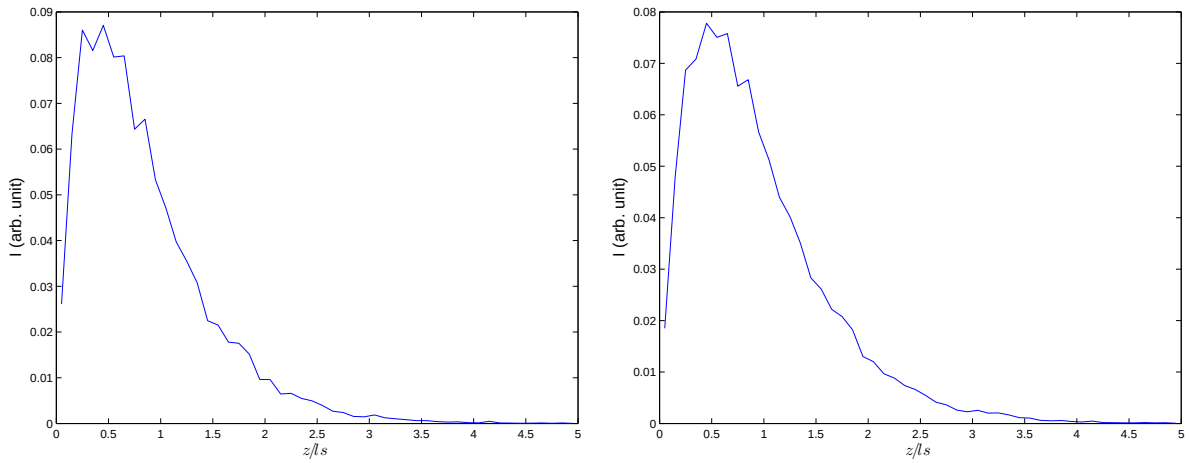

(a) (b)

Figure 8. The distribution of photons of penetration depth $z_{\max}$ for backscattered double scattering low coherence light of parallel polarization in the exact backscattering direction. (a) $L_c = 0.01l_s$ and (b) $L_c = 0.1l_s$.

4. DISCUSSION AND CONCLUSION

In summary, we have presented a novel Electric field Monte Carlo approach for directly simulating coherent backscattering of coherent or partially coherent polarized light. The strong dependence of CBS on the polarization state of light has been demonstrated. The penetration depth of low coherence backscattering light has also been investigated using the EMC approach. EMC simulations on partially coherent light backscattering from a human epithelial tissue model show that the penetration depth of low coherence light can be reduced to the level of one scattering length under illumination by a source of an extreme low spatial coherence. The penetration depth less than one scattering length, however, has not been obtained even when the spatial coherence length is reduced to $0.01l_s$. This finding is contrary to the conventional assumptions.[10] This calls for a careful interpretation of the penetration depth for low coherence backscattering techniques applied to tissue diagnostics. A theoretical investigation to understand the observed phenomenon is underway.

ACKNOWLEDGMENTS

This work is supported by Cottrel College Science Award.

REFERENCES

1. Y. Kuga and A. Ishimaru, "Retroreflection from a dense distribution of spherical particles," *J. Opt. Soc. Am. A* **1**, pp. 831–835, 1984.
2. M. P. V. Albada and A. Lagendijk, "Observation of weak localization of light in a random medium," *Phys. Rev. Lett.* **55**, pp. 2692–2695, Dec. 1985.
3. P.-E. Wolf and G. Maret, "Weak localization and coherent backscattering of photons in disordered media," *Phys. Rev. Lett.* **55**(24), pp. 2696–2699, 1985.
4. R. Lenke, R. Tweer, and G. Maret, "Coherent backscattering of turbid samples containing large Mie spheres," *J. Opt. A: Pure Appl. Opt.* **4**, pp. 293–298, 2002.
5. M. Xu, "Electric field Monte Carlo for polarized light propagation in turbid media," *Opt. Express* **12**, pp. 6530–6539, 2004. `http://www.opticsexpress.org/abstract.cfm?URI=OPEX-12-26-653`.
6. K. G. Phillips, M. Xu, S. K. Gayen, and R. R. Alfano, "Time-resolved ring structure of circularly polarized beams backscattered from forward scattering media," *Opt. Express* **13**, pp. 7954–7969, 2005.
7. M. Xu and R. R. Alfano, "Random walk of polarized light in turbid media," *Phys. Rev. Lett.* **95**, p. 213905, 2005.
8. D. S. Saxon, "Tensor scattering matrix for the electromagnetic field," *Phys. Rev.* **100**(6), pp. 1771–1775, 1955.
9. M. Born and E. Wolf, *Principle of Optics–Electromagnetic Theory of Propagation, Interference and Diffraction of Light*, Pergamon Press, 6th ed., 1980.
10. Y. L. Kim, V. M. Turzhitsky, Y. Liu, H. K. Roy, R. K. Wali, H. Subramanian, P. Pradhan, and V. Backman, "Low-coherence enhanced backscattering: review of principles and applications for colon cancer screening," *J. Biomed. Opt.* **11**(4), p. 041125, 2006. (9 pages).
11. J. Sawicki, N. Kastor, and M. Xu, "Electric field monte carlo simulation of coherent backscattering of polarized light by a turbid medium," *Opt. Express* , 2007. (to be submitted).
12. M. Xu and R. R. Alfano, "Fractal mechanisms of light scattering in biological tissue and cells," *Opt. Lett.* **30**, pp. 3051–3053, 2005.
13. T. T. Wu, J. Y. Qu, and M. Xu, "Unified Mie and fractal scattering by biological cells and subcellular structures," *Opt. Lett.* **32**, pp. 2324–2326, 2007.
14. M. Xu, T. T. Wu, and J. Y. Qu, "Unified mie and fractal scattering by cells and experimental study on application in optical characterization of cellular and subcellular structures," *J. Biomed. Opt.* , 2007. (in press).
15. T. Collier, M. Follen, A. Malpica, and R. Richards-Kortum, "Sources of scattering in cervical tissue: determination of the scattering coefficient using confocal microscopy," *Appl. Opt.* **44**, pp. 2072–2081, 2005.
16. J. Qu, C. MacAulay, S. Lam, and B. Palcic, "Optical properties of normal and carcinomatous bronchial tissue," *Appl. Opt.* **33**, pp. 7397–7405, 1994.